ELSEVIER

Biophysical Chemistry 89 (2001) 35–51

Biophysical Chemistry

www.elsevier.nl/locate/bpc

Intracellular Mg^{2+} diffusion within isolated rat skeletal muscle fibers

Jean Claude Bernengo[a], Claude Collet[b], Vincent Jacquemond[b,*]

[a] *Centre Commun de Quantimétrie, Université Claude Bernard Lyon 1, 8, avenue Rockefeller, 69373 Lyon, France*
[b] *Laboratoire de Physiologie des Eléments Excitables, Université Claude Bernard Lyon 1, ERS CNRS 2019, 43 boulevard du 11 novembre 1918, F69622 Villeurbanne, France*

Received 4 August 2000; received in revised form 28 September 2000; accepted 28 September 2000

Abstract

Intracellular free magnesium concentration ($[Mg^{2+}]_i$) was measured in enzymatically isolated rat skeletal muscle fibers using the fluorescent dye mag-indo-1. The change in $[Mg^{2+}]_i$ produced by a local intracellular microinjection of magnesium pidolate (magnesium pyrrolidone carboxylate) was measured at a given distance from the injection site. In one series of experiments this protocol was tested on isolated fibers that were completely embedded into silicone grease: under these conditions, the injection produced an increase in $[Mg^{2+}]_i$ that reached a steady level some time following the injection. The time-course of the $[Mg^{2+}]_i$ change could be well accounted for by a model of longitudinal diffusion. The mean apparent Mg^{2+} diffusion coefficient (D_{app}) was 188 ± 9 μm^2 s^{-1} ($n = 16$), approximately four times lower than the value measured in vitro. This reduction likely results from the effects of cytoplasmic viscosity and of Mg^{2+} binding to low affinity static sites. Another series of measurements was performed on fibers that were either partially or completely free of silicone: under these conditions, the time course of the change in $[Mg^{2+}]_i$ was in many cases more complex than predicted by simple diffusion.

Keywords: Intracellular free magnesium; Diffusion; mag-indo-1; Mammalian skeletal muscle

* Corresponding author. Physiologie des Eléments Excitables, Université Claude Bernard Lyon 1, ERS CNRS 2019, Bât. 401 B, 43 boulevard du 11 novembre 1918, F69622 Villeurbanne, France. Tel.: +33-4-72-43-10-32; fax: +33-4-78-94-68-20.
E-mail address: vincent.jacquemond@univ-lyon1.fr (V. Jacquemond).

0301-4622/01/$ - see front matter
PII: S0301-4622(00)00215-5

1. Introduction

Intracellular free magnesium plays a fundamental role in regulating the activity of numerous enzymes and ion channels in various cell types (for review, see [1,2]). In skeletal muscle, the $[Mg^{2+}]_i$ level is likely to influence different steps of the excitation–contraction coupling process (see for instance [3]). However, the membranous and intracellular mechanisms involved in the regulation of $[Mg^{2+}]_i$ are far from being well understood. For instance, in frog skeletal muscle, it seems that elevation of extracellular magnesium influences $[Mg^{2+}]_i$ only on a very slow time scale suggesting either a very low Mg^{2+} membrane permeability, or the presence of an efficient transmembranous Mg^{2+} transport system that remains to be identified [4]. Along this line, data concerning the potential role of a transmembrane Mg^{2+} transport, Na^+-gradient-driven remain controversial [4,5]. From a more general point of view, there is thus strong interest in gaining information about Mg^{2+} behavior and properties within the intracellular environment. In a previous study, we demonstrated the effectiveness of the fluorescent dye mag-indo-1 for measuring $[Mg^{2+}]_i$ in isolated skeletal muscle fibers at rest, and the changes in $[Mg^{2+}]_i$ driven by a Mg^{2+} entry through the plasma membrane [6]. In the present study, we measured the change in $[Mg^{2+}]_i$ induced by intracellular microinjection of a magnesium salt in isolated rat skeletal muscle fibers that were completely embedded into silicone grease. Experiments were performed so as to measure longitudinal diffusion of $[Mg^{2+}]_i$ allowing determination of its apparent intracellular diffusion coefficient. Determination of this parameter is of particular importance as it should, for instance, give insights into the properties of the myoplasmic compartment in terms of Mg^{2+} binding and/or Mg^{2+} sequestration mechanisms. At this point, it should be mentioned that, while the intracellular diffusion properties of Mg^{2+} ions remain so far obscure, there has been experimental and theoretical studies which addressed the problem of Ca^{2+} diffusion within the cytoplasm of various cell types: more specifically, several lines of work pointed out the complexity of this phenomenon, due in particular to the interactions between Ca^{2+} and fixed and mobile ligands within the cytoplasm [7–9]. Also, it has been clearly established that, when using an ion-selective optical probe for Ca^{2+} diffusion measurements, the affinity of the probe for Ca^{2+} and the diffusion coefficient of the probe are of critical importance, since the diffusion velocity of Ca^{2+} will be different whether it is free or bound to the probe. Such reversible binding can either increase or decrease the ion diffusion speed depending on the relative diffusion coefficients of the ion and probe [10], and such effects had to be considered within the present work.

Finally, apart from measuring the intracellular Mg^{2+} diffusion rate in silicone-embedded fibers, we also attempted to study the potential ability of the fibers to regulate a cytoplasmic $[Mg^{2+}]$ rise under more physiological conditions, by performing the same type of measurements on fibers that were either partially or completely free of silicone.

2. Materials and methods

The methods used here for $[Mg^{2+}]$ measurements were similar to those previously described [6] except that rat muscle fibers were used instead of mouse. All experiments were performed at room temperature (20–22°C).

2.1. Isolation and preparation of the skeletal muscle fibers

All experiments were performed in accordance with the guidelines of the French Ministry of Agriculture (87/848) and of the European Community (86/609/EEC). We used intact skeletal fibers isolated from the flexor digitorum brevis (fdb) muscles of Sprague–Dawley male rats (*Rattus norvegicus*). Rats were killed by an overdose administration of sodium pentobarbital, and fdb muscles were removed. Single fibers were isolated from collagenase (Sigma type 1) treated muscles as previously described [11]. The mean length and

diameter of the fibers that were used in the present study were 1230 ± 60 μm and 45 ± 2 μm ($n = 29$), respectively.

When fibers were to be partially or fully embedded into silicone grease, the bottom of the experimental chamber, which consisted of a glass coverslip, was covered with a thin layer of that material (silicone grease 70428; Rhône-Poulenc, Saint Fons, France). The chamber was then filled with culture medium containing 10% bovine fetal serum (MI199, Eurobio, France) and the Collagenase treated muscles were gently triturated within the chamber through the cut disposable tip of a Pipetman. After ~10 min, the culture medium was replaced by Tyrode solution. Fibers where then either partially or completely embedded into silicone grease using a previously described procedure [6,11]. These fibers will be referred to as 'partially insulated' and 'fully insulated', respectively. Intracellular dye loading was then performed by local pressure microinjection of a solution containing mag-indo-1 (pentapotassium salt, Molecular Probes Inc., Eugene, OR, USA) dissolved at a concentration of 1.1 mM in an intracellular-like solution (see Section 3.6), using a Picospritzer II apparatus (General Valve Corp., Fairfield, NJ, USA). The tip of the injecting micropipette was inserted through the silicone grease, within one end of an isolated silicone-embedded fiber. A dye microinjection was usually performed at both ends of each fiber, except for the experiments designed to measure dye diffusion for which a single injection was performed within one end of the muscle fibers. Fibers were then left for ~60 min until the dye was homogeneously distributed within the fibers. For partially insulated fibers, only a portion at both ends of the isolated fibers was embedded into silicone so that a large part of the fiber's length (45–70%) was free. In these fibers, a dye microinjection was also performed within the two silicone-insulated end portions of the fibers.

For measurements performed on fibers that were completely free of silicone, the coverslip at the bottom of the chamber was coated with poly-L-lysine (Sigma) at 0.1% to favor adherence of the fibers. Again, a dye microinjection was performed at both ends of each fiber. These experiments were more difficult than in fully insulated and partially insulated fibers because silicone-free fibers also had to undergo three microinjections (including the Mg-pidolate one) which in some cases produced local damage and subsequent contracture of the fibers. Only fibers that did not show any sign of damage at the injection sites were kept for analysis.

3. Measurement of Mg^{2+} diffusion within the fibers

Following intracellular dye equilibration, fibers were locally pressure microinjected with an injectable solution of Mg-pidolate (337 mM magnesium pyrrolidone carboxylate, Mag-2, Rhône-Poulenc Rorer, Paris, France). Mg-pidolate was used rather than any other more classical magnesium salt for the following reasons. First, chloride was not used because, since a large concentration of a magnesium salt was to be present at the injection site, we wanted to avoid any possible effect of a high intracellular chloride level (diffusing rapidly within the fiber), on the putative mechanisms of Mg^{2+} transport and regulation. Also we wanted to use a non permeant anionic specie in order to prevent any possible consequence of Cl^- transport across the plasma membrane on intracellular Mg^{2+} regulation. Pidolate was used because of its high molecular weight and thus low mobility, and also because it is used in human therapeutics and was thus expected to have no toxic effect on the muscle fibers. The injection was always performed with the pipette inserted within one near-end of the fiber. Care was taken to maintain the injection duration as short as possible (typically less than 5 s). When the injection was completed, the pipette was removed and fluorescence measurements were taken at regular time intervals at a set distance (usually between 200 and 800 μm) from the magnesium injection site. The length and diameter of the fibers and the distance between injection site and fluorescence detection site were measured with an eyepiece micrometer.

3.1. Measurements and calibration of mag-indo-1 fluorescence signals

The optical set-up used for fluorescence measurements was described previously [6,11,12]. The light beam from a high pressure mercury bulb placed on the top of a Nikon Diaphot epifluorescence microscope, went through a 335-nm interference filter for mag-indo-1 excitation, and was focused onto the preparation through a quartz aspherical doublet. The emitted fluorescence light was collected by the 40 × objective and detected at 405 (F_{405}) and 470 nm (F_{470}) with a 10-nm bandwidth by two photomultipliers. Fluorescence signals were digitized and stored on disk using a commercial software (Biopatch Acquire, Bio-logic, Claix, France) driving an A/D, D/A converter (Lab Master DMA board, Scientific Solutions Inc., Solon, OH, USA). The fluorescence measurement field was 40 μm in diameter. Mag-indo-1 microinjected fibers were only UV illuminated while taking measurements in order to minimize photobleaching. Cell autofluorescence was negligible and not different from the fluorescence measured when no cell was present in the field. Background fluorescence at both emission wavelengths was measured next to each tested fiber and then subtracted from all measurements.

The $[Mg^{2+}]$ and/or mag-indo-1 percent saturation were calculated from the ratio (R) of the background corrected fluorescence at 405 and 470 nm (F_{405}/F_{470}) as previously described [6] using the standard procedures developed by Grynkiewicz et al. [13], with the parameters R, R_{min} (R in absence of Mg), R_{max} (R in presence of a saturating Mg concentration), K_D (the apparent binding constant for the mag-indo-1-Mg complex) and the ratio of F_{470} in absence of Mg to F_{470} in presence of a saturating Mg concentration. The value for K_D was assumed to be equal to 5.1 mM [6]. Values for R_{min} and R_{max} were determined from fully insulated, mag-indo-1 loaded fibers that were microinjected either with a solution containing 100 mM K_2-ATP, 5 mM Hepes, pH 7.20, or 1 M $MgCl_2$, respectively. Mean values for R_{min} and R_{max} were 0.31 ± 0.04 ($n = 6$) and 2.72 ± 0.1 ($n = 17$). The value of the ratio of F_{470} in the absence of Mg to F_{470} in the presence of a saturating Mg concentration was calculated as previously described [6] from the slope of plots of F_{470} vs. F_{405} measured while $[Mg^{2+}]_i$ was increasing following Mg-pidolate injection. This gave a mean value of 2.8 ± 0.1 ($n = 27$).

3.2. Modeling of Mg^{2+} longitudinal diffusion within the muscle fiber

3.2.1. Principles

An ion migrates within a cell under the influence of diffusion forces derived from its local chemical potential (passive transport) and can bind to any fixation site according to its affinity. Both processes are of stochastic nature and occur simultaneously. In addition some ligands may be mobile, leading to transport of the bound ion through ligand diffusion. In order to get a concentration profile $C(x,y,z,t)$ of the migrating ion in any point of a given closed volume at time t following a perturbation, a set of differential equations taking into account both diffusion (Fick's second law) and binding kinetics has to be solved, either analytically or numerically. Crank was the pioneer in such studies and presented analytical solutions of Fick's second law under different geometrical and perturbating conditions (see [14]). He also considered diffusion and simultaneous binding of the ion to a non-mobile buffer, and showed that, provided that the ion diffusion coefficient D is replaced by an apparent ion diffusion coefficient D_{app}, Fick's law remains valid.

In their study concerning Ca^{2+} diffusion, Wagner and Keizer [10] started from general diffusion and ionic equilibrium equations. They took into account mobile ligands and obtained a second order differential equation analogous to Fick's law. This also led to the definition of an apparent diffusion coefficient D_{app} which depends on the concentrations, equilibrium constants and diffusion coefficients of the Ca^{2+} ligands. A non-diffusive term involving the square of the calcium gradient produces a transient effect, mostly important at the time of injection, and which then rapidly vanishes. This model gave a very general differential equation for the concentration profile. However, some assumptions had to be made

in order to obtain analytical solutions: in particular, geometrical considerations such as axial symmetry and transversally uniform distribution of the moving ions and ligands, and also binding kinetics that would be much faster than diffusion processes, i.e. instantaneous at the diffusion time scale.

Using the same assumptions, Zador and Koch [15] showed that there is a good analogy between diffusion and electrical conduction in a leaky cable. The axial diffusion of Ca^{2+} could then be treated as an ionic current by applying the classical cable equations. Though based on a different approach, this model led to similar formal results as in Wagner and Keizer [10]: a diffusive term defining D_{app}, and a non-diffusive transient term vanishing with the Ca^{2+} gradient.

The following derivation takes advantage of the fact that, under our experimental conditions, the non-diffusive term can be neglected very soon after Mg^{2+} injection. As a consequence, Fick's law can be applied with $D = D_{app}$. Therefore, we refined the geometry of the simple diffusion model (along the main cylinder axis of the cell) by considering a finite layer of injected ions, reflection on the fiber's ends and by integrating the concentration $C(x,t)$ over the observation volume. The relationship between D_{app} and the true cytoplasmic Mg^{2+} diffusion coefficient D_{Mg} (in the absence of any Mg^{2+} binding) will be considered in Section 5.

The muscle was considered as a homogeneous cylinder of length l and radius r, and was assumed to be longitudinally and radially isotropic. The ends and walls of the cylinder were assumed to be fully reflective. As magnesium injection was performed at one end of the cylinder, the initial conditions right after the end of the injection were assumed to correspond to an end section of fiber of length h, uniformly filled with Mg^{2+} ions at a given molar concentration C_0. The fluorescence intensity of the dye was measured perpendicularly to the cylinder axis at a distance d from the injection site, in a section of radius w equal to 20 μm, over which the Mg^{2+} and dye concentrations are averaged. This section actually corresponds to a volume V defined by the intersection of the optical collection figure (rather conical but assumed to be a cylinder of vertical axis and of radius w) with the cell cylinder.

The diffusion model along the main cylinder axis relied on Fick's law with an extended initial distribution.

We considered a homogeneous layer of Mg^{2+} ions, ranging from $x = -h$ to $x = h$, starting to diffuse at $t = 0$ towards both sides of the cylinder. The layer can be divided into an infinity of elementary sheets of thickness dh. At any point x of the cylinder axis, the concentration $C(x,t)$ can be calculated as the sum of these elementary sheets contribution (see [15] for details).

After integration, this process gives Eq. (1):

$$C(x,t) = \frac{C_0}{2}\left\{ erf\left(\frac{h-x}{2\sqrt{(D\times t)}}\right) + erf\left(\frac{h+x}{2\sqrt{(D\times t)}}\right)\right\} \quad (1)$$

In this expression, D is the translational diffusion coefficient, and will be referred to as D_{app} when describing and interpreting experimental data. The *erf* function is defined as usual:

$$erf(z) = \frac{2}{\sqrt{\pi}} \times \int_0^z \exp(-\eta^2) \times d\eta \quad (2)$$

According to the total reflection on the microinjected cell end at $x = 0$, the actual diffusion profile is obviously the same as above, since this reflection leads to the superposition of two identical diffusing profiles.

The concentration $C(t)$ averaged over the observation volume V centered at a distance d from the origin was computed through integration of $C(x,t)$ inside this volume:

$$C(t) = \frac{1}{V} \times \int_{-W}^{W} C(d+y) \times S(y) \times dy \quad (3)$$

The last important step was to take into account the end effects. The procedure consisted in considering any membrane reflection as a reflection on a boundary at which the concentration is maintained, while the sign of the movement is

changed. Therefore, at the site of measurement, the actual concentration is the algebraic sum of all the contributions from incoming and reflected waves.

Mathematically, these contributions correspond to a series of terms such as Eq. (1), in which $(h-x)$ and $(h+x)$ are replaced by $(h-2kl-x)$ and $(h+2kl+x)$, k being an integer between 0 and infinity.

$$C(x,t) = \frac{C_0}{2}\Sigma\left[erf\left(\frac{h-(2\times k\times l)-x}{2\sqrt{(D\times t)}}\right) + erf\left(\frac{h+(2\times k\times l)+x}{2\sqrt{(D\times t)}}\right)\right] \quad (4)$$

In practice, however, the *erf* terms vanish for high k values, and the computation was stopped when corrective terms did not contribute to more than 1% of the total $C(t)$ term (the shorter the cell length l, the higher the number of terms, $n=5$ being a maximum).

The whole calculation is rather complicated, since, instead of Eq. (1), the above series has to be inserted in the numerical computation of integral (3) for each step of the Romberg procedure. It was computed in PASCAL, and operated on a Pentium II processor.

3.3. Determination of the diffusion parameters

For a given experiment, the known parameters are the fiber length l, the distance from injection point to observation center d, and the radius of the observation cylinder w, as illustrated in Fig. 1. The unknowns are D and h, which have to be determined from the experimentally measured Mg^{2+} concentration recorded at increasing times after injection, through an adjustment procedure. The actual value of h has to depend on the extent to which the pipette Mg^{2+} concentration gets diluted within the injected portion of fiber. For the calculation, the dilution factor was assumed to be 1.5, and the amount of Mg^{2+} taken up by intrinsic buffers was neglected. This means that the determined value of h corresponded to the cell length multiplied by the ratio of the change

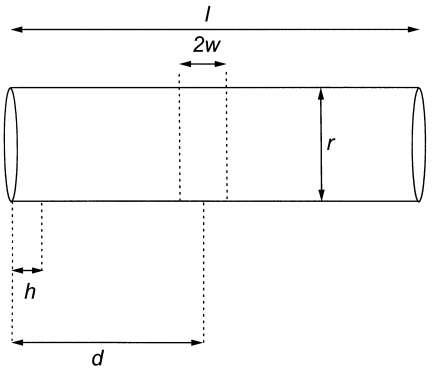

Fig. 1. Schematic representation of the parameters used for diffusion modeling. The fiber is considered as a cylinder of length l and radius r. w is the radius of the fluorescence measurement cylinder. Injection is achieved within one end of the fiber. d is the distance from injection point to observation center and h is the length of fiber section assumed to be uniformly filled with the injected solution (see text for details).

in $[Mg^{2+}]$ at infinite time, to the initial $[Mg^{2+}]$ (assumed to be 220 mM) within the injected portion of fiber. In the fully insulated fibers, this led to a mean value of 37 ± 5 μm ($n=16$). Simulations showed that, under our most typical experimental conditions where the distance between Mg^{2+} injection site and $[Mg^{2+}]$ measurement site was larger than 500 μm, the time course of $[Mg^{2+}]$ diffusion would be very little affected if, for instance, our assumptions had led to a five times underestimation of the value of h (not illustrated).

Due to the complex non analytical relationship between the experimental data and the computed concentrations, a straightforward adjustment algorithm based on non-linear curve fitting could not reasonably be envisaged, and, after many trials, a semi-automatic determination of the best fitting values was carried out. The iterations were partly integrated in the calculation program, while the final adjustment of the theoretical function to the experimental data points was sought for by hand.

3.4. Measurement and modeling of mag-indo-1 and Ca^{2+} diffusion within the fibers

In a few experiments, we attempted to estimate

the dye and Ca^{2+} diffusion coefficients within fully silicone-insulated muscle fibers, using the above described model. For dye diffusion, we measured the fluorescence at both wavelengths (405 and 470 nm) at regular time intervals following dye microinjection. As for Mg^{2+} diffusion experiments, measurements were taken at a given distance from the injection site. Since none of the two wavelengths were isosbestic for magnesium, the estimation of the dye diffusion coefficient with the model required assuming that no $[Mg^{2+}]_i$ change occurred during the diffusion process and that the amount of injected volume did not interfere with the time course of dye diffusion. No attempt was done to calibrate the levels of fluorescence in terms of actual dye concentration, and the changes in fluorescence data were scaled to an arbitrary value.

For Ca^{2+} diffusion experiments, fibers were pressure microinjected with a pipette containing indo-1 (0.5 mM in the same intracellular-like solution as mag-indo-1). After dye equilibration, the end of a fiber was microinjected with the intracellular-like solution to which 20 mM $CaCl_2$ was added and fluorescence measurements were then taken at a given distance from the injection site. $[Ca^{2+}]_i$ estimates were done using previously described procedures [11]. The $CaCl_2$ microinjection inevitably produced a local contracture at the injection site, but the silicone insulation allowed maintenance of the fiber integrity.

3.5. In vitro measurements of mag-indo-1 and Mg^{2+} diffusion

In vitro measurements were performed on the experimental set up, using glass capillary tubes 40–60 μm in diameter. The experimental procedure for measuring diffusion was similar to the one used for skeletal muscle fibers.

For measurements of mag-indo-1 diffusion, capillaries were filled with the intracellular-like solution and immerged within the silicone layer covering the bottom of the chamber. The tip of a micropipette filled with 1.1 mM mag-indo-1 dissolved in the intracellular-like solution was then inserted within one opened end of the capillary, through the silicone layer, and a short pressure pulse was applied. Fluorescence measurements were then taken at regular intervals, at a set distance from the capillary end.

For measurements of Mg^{2+} diffusion, the same procedure was applied, except that capillary tubes were filled with mag-indo-1 (0.1 mM in the intracellular-like solution) and the micropipette contained the Mg-pidolate solution. In vitro values for R_{min} and R_{max} were obtained from capillary tubes containing 0.1 mM mag-indo-1 in a high EDTA and high Mg^{2+} containing solution, respectively. The in vitro value for the ratio of F_{470} in the absence of Mg to F_{470} in the presence of a saturating Mg concentration was calculated from the slope of plots of F_{470} vs. F_{405} measured while $[Mg^{2+}]$ was increasing.

3.6. Solutions

Tyrode solution contained (mM): 140 NaCl, 5 KCl, 2.5 $CaCl_2$, 2 $MgCl_2$, 10 HEPES, adjusted to pH 7.20 with NaOH. Intracellular-like solution contained: 120 K-glutamate, 5 Na_2-ATP, 5 Na_2-phosphocreatine, 5.5 $MgCl_2$, 5 glucose, 5 HEPES adjusted to pH 7.20 with K-OH.

3.7. Statistics

Least-squares fits were performed using a Marquardt–Levenberg algorithm routine included in Microcal Origin (Microcal software Inc., Northampton, MA, USA). Data values are presented as means ± S.E.M.

4. Results

4.1. Mg^{2+} diffusion in fully silicone-embedded skeletal muscle fibers

Fig. 2 shows the time-dependent changes in mag-indo-1 fluorescence (top row) and in the corresponding mag-indo-1 percent saturation (middle row) and $[Mg^{2+}]$ (bottom row) due to a Mg-pidolate injection in fully insulated, intact skeletal muscle fibers. Data shown in a and b were taken from two distinct fibers, respectively. The first data point from each series corresponds

to the value at the measurement site before magnesium injection was performed. In Fig. 2, both fibers were 1600 μm long and the fluorescence measurement site was 750 μm away from the magnesium injection site. Magnesium injection was followed by a slow rise in F_{405} together with a simultaneous drop in F_{470}, in agreement with what was expected from an increase in $[Mg^{2+}]_i$ (see [6]). The time course of relative change in fluorescence was not identical at both wavelengths: F_{405} increased to a more or less steady level followed by a fairly slight decrease some time after the injection, while F_{470} kept decreasing over the same period. This was likely due to dye photobleaching, the effect of which was taken care of by ratioing the fluorescence data, as shown by the corresponding mag-indo-1 percent saturation (and $[Mg^{2+}]_i$) which ended up reaching a stable steady level late after the injection. In Fig. 2a, $[Mg^{2+}]_i$ rose from an initial level of ~1.3 mM to ~4.6 mM while in Fig. 2b the change in $[Mg^{2+}]_i$ was approximately twice as large, increasing from ~2.1 mM to ~7.8 mM. As the two fibers were similar in size (fiber diameter was 48 μm and 43 μm in Fig. 2a,b, respectively), the most likely explanation for this difference was that the amount of fiber volume that was injected with magnesium was larger in the fiber shown in Fig. 2b than in the one shown in Fig. 2a.

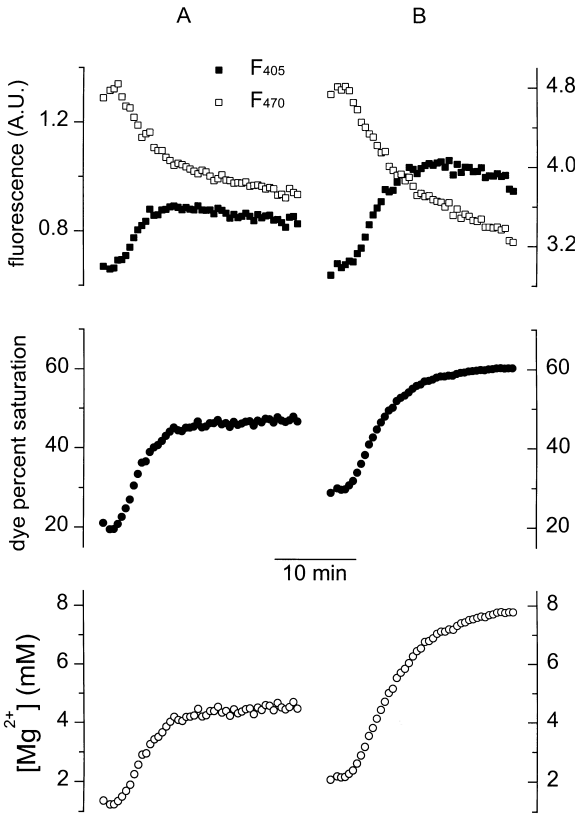

Fig. 2. Effect of a magnesium injection on mag-indo-1 fluorescence (top row), corresponding mag-indo-1 percent saturation (middle row) and $[Mg^{2+}]_i$ (bottom row) in two distinct fully insulated fibers (panels a and b, respectively). Both fibers were 1600 μm long and the distance d between injection site and fluorescence measurement center was 750 μm. On the top row, filled and open symbols correspond to the background corrected fluorescence at 405 nm and 470 nm, respectively, in arbitrary units (A.U.).

4.2. Modeling of Mg^{2+} diffusion in fully embedded muscle fibers

The two panels in Fig. 3 present $[Mg^{2+}]_i$ changes induced by a Mg-pidolate injection in two fully embedded muscle fibers, respectively. The continuous line superimposed to the data points corresponds to the best fit of the diffusion model to the experimental data. It was achieved by setting the values for the apparent magnesium diffusion coefficient (D_{app})and for the length of fiber portion that was injected (h) as described in Section 2. In Fig. 3a, the curve was calculated with a D_{app} value of 200 $\mu m^2\ s^{-1}$. In Fig. 3b, the value for D_{app} was 210 $\mu m^2\ s^{-1}$. In Fig. 3a,b, the full length of the two fibers was 1200 μm and 1780 μm, respectively, and in both cases, the distance between the injection site and the measurement site was 750 μm. In each panel, the inset shows an enlarged view of the same data, focused onto the first 5 min following the injection. The dashed curves correspond to the diffusion profiles calculated with a change in D_{app} of +10% (upper curve from the data points) or −10% (curve lower than the data points). Results show that under these experimental conditions, the time-course of the $[Mg^{2+}]_i$ change could adequately be reproduced by Mg^{2+} diffusion within the cytoplasm with no additional assumption. It

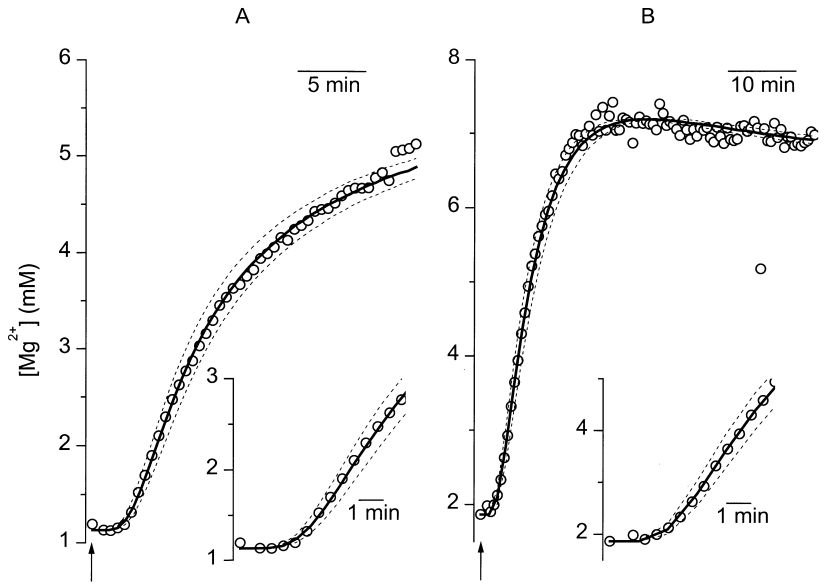

Fig. 3. Result from modeling Mg^{2+} diffusion in two distinct fully insulated fibers (a and b, respectively). Open circles correspond to the measured $[Mg^{2+}]_i$. Arrows point to the value measured before Mg-pidolate injection was performed. In a and b, the superimposed continuous lines show the calculated diffusion profile with a D_{app} of 200 $\mu m^2\ s^{-1}$ and 210 $\mu m^2\ s^{-1}$, respectively. Corresponding values for h were 23 μm and 38 μm, respectively. In each panel, the dotted curves show the diffusion profiles calculated with a change of −10% (curve lower than the data points) and +10% (curve upper from the data points) of the value of D_{app}. In a and b, fiber length was 1200 μm and 1780 μm, respectively, and the distance d between injection site and measurement site was 750 μm. In both panels, the inset shows an enlarged view of the first data points and associated modeled diffusion profiles.

can also be noted that in panel b of Fig. 3, after reaching a maximum value of ~7 mM, $[Mg^{2+}]_i$ tended then to slowly decrease. Such a slow late $[Mg^{2+}]_i$ decrease was clearly observed and predicted by the model when the distance between the measurement site and the injection site was shorter than half the full length of the fiber. This phenomenon is clearly illustrated in Fig. 4a which shows the result of a Mg^{2+} diffusion experiment, for which the distance between injection site and fluorescence measurement site corresponded to ~25% of the full length of the fiber. It should also be mentioned that in fully insulated fibers, $[Mg^{2+}]_i$ reached an elevated level that remained steady even at late time following the injection. This is illustrated in Fig. 4b where $[Mg^{2+}]_i$ was followed for approximately 2 h after the injection. The graph presented in Fig. 5 shows the amplitude distribution of D_{app} from 16 experiments similar to the ones illustrated in Figs. 2–4. There was little scattering in the distribution and the mean D_{app} value was $188 \pm 9\ \mu m^2\ s^{-}1$ ($n = 16$). There was no correlation between the value of D_{app} and the resting $[Mg^{2+}]$ level within the measured range (1–5 mM, mean value of 2.4 ± 0.4 mM). A linear fit to a plot of the value of D_{app} vs. resting $[Mg^{2+}]_i$ gave a slope of $-3\ \mu m\ s^{-1}\ mM^{-1}$ and a correlation coefficient of −0.15 (not illustrated). There was no more correlation between the value of D_{app} and the value of any other measured parameter such as the length and diameter of the fiber, the distance between injection and measurement site, and the maximum $[Mg^{2+}]$ level reached during the experiment (data not shown). The mean maximum change in $[Mg^{2+}]_i$ measured from this series of fibers was 7.2 ± 1 mM. If we were to assume that, right after the injection, 330 mM Mg^{2+} was present within a definite end portion of the full length of the fibers, it would correspond to a mean injected

volume of $2.8 \pm 0.6\%$ of the total volume of fiber. Of course, this estimation holds true only if all of the injected Mg^{2+} is assumed to be diluted into the entire volume of fiber without any buffering and/or extrusion from the cytoplasmic compartment. It may be noticed that the mean resting $[Mg^{2+}]_i$ measured here was larger (2.4 ± 0.4 mM, $n = 16$) than found in a previous study [6] in mouse skeletal muscle fibers (1.5 ± 0.2 mM, $n = 7$). This higher mean value results from four fibers which displayed resting $[Mg^{2+}]$ levels higher than 3 mM. Excluding these four values would give a mean resting Mg^{2+} level of 1.6 ± 0.1 mM ($n = 12$) a value that is much closer to the previously published one. The reasons for which these fibers displayed a high resting Mg^{2+} level are unclear. We cannot rule out the possibility that they were either in somewhat hypoxic conditions, or that they were damaged during the isolation procedure. However, in the absence of any other experimental indication of such possibilities, this remains speculative and the results from these fibers were thus kept for analysis.

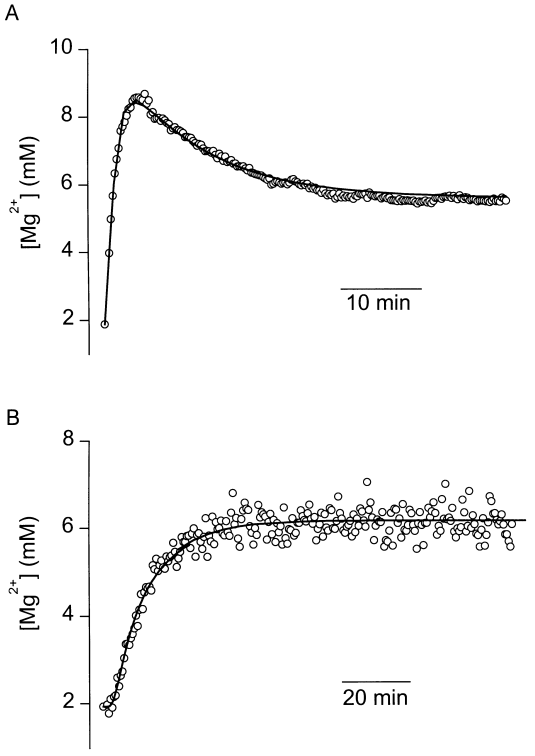

Fig. 4. Changes in $[Mg^{2+}]_i$ (open circles) and corresponding calculated diffusion profiles (superimposed continuous curves) in two fully insulated fibers. In panel a, after reaching a peak, $[Mg^{2+}]_i$ decreased to a sustained elevated level due to the short distance between injection site and measurement site ($d = 275$ μm) as compared to the length of the fiber ($l = 1075$ μm). Panel b illustrates stability over ~2 h of the elevated $[Mg^{2+}]_i$ level reached after a Mg-pidolate injection. Fiber length was 1150 μm and d was 750 μm. In a and b, diffusion profiles were calculated with D_{app} values of 191 $\mu m^2\ s^{-1}$ and 180 $\mu m^2\ s^{-1}$, and h values of 18 μm and 22 μm, respectively.

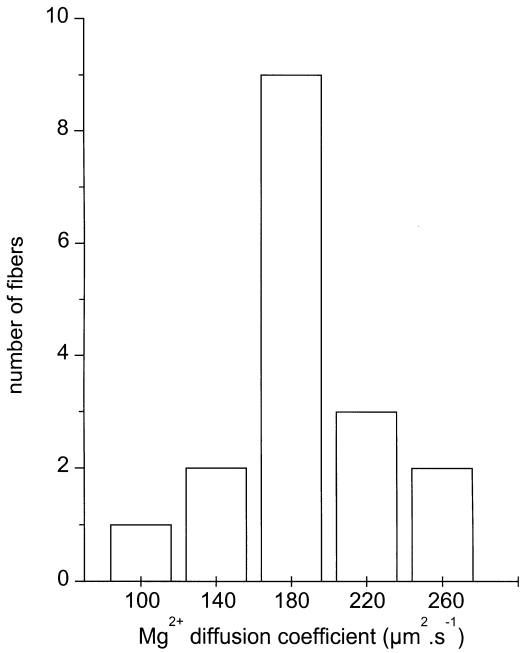

Fig. 5. Distribution of the values of D_{app} in fully insulated fibers. Diffusion coefficients estimated from fitting the diffusion model to changes in $[Mg^{2+}]_i$ measured in distinct fibers, were sorted with a 40-$\mu m^2\ s^{-1}$ increment.

4.3. Mg^{2+} diffusion in partially insulated fibers and in silicone-free fibers

Since experiments performed on fully insulated fibers showed that the time course of the Mg^{2+} change induced by a magnesium injection could be well accounted for by simple Mg^{2+} diffusion along the fiber, a series of measurements was performed in fibers that were either left partially

free of silicone or completely free of silicone (see Section 2). Our goal was to test the possibility that, under more physiological conditions, we would be able to detect signs of operating of a $[Mg^{2+}]_i$ regulatory mechanism. In this case, we were ready to expect that the time course of the $[Mg^{2+}]$ change due to a microinjection would be more complex than observed in fully insulated fibers (see above). Fig. 6 illustrates results from $[Mg^{2+}]_i$ measurements following a Mg-pidolate injection, taken either from partially insulated fibers (Fig. 6a) or from fibers that were completely free of silicone (Fig. 6b). In both series, there was obviously no way we could qualify any result of 'typical' as the pattern of evolution of $[Mg^{2+}]_i$ varied considerably from fiber-to-fiber. In this respect, our expectations were fulfilled as the time course of change in $[Mg^{2+}]_i$ was in many cases not conform to simple diffusion. The time-dependent evolution of the change in $[Mg^{2+}]_i$ was, however, unpredictable. Out of nine partially insulated fibers, the initial $[Mg^{2+}]_i$ increase was followed by a slow decay in two fibers as exemplified on the first row of Fig. 6a. In four partially insulated fibers, the change in $[Mg^{2+}]_i$ reached a steady level and its time course could be well adjusted using the diffusion model as illustrated on the second row of Fig. 6a. Finally, in three partially insulated fibers, an initial rise in $[Mg^{2+}]_i$, the time course of which was consistent with the diffusion model, was followed by a totally unexpected secondary slower rising phase (as exemplified in the third row of Fig. 6a). In Fig. 6, the curves superimposed to the data points correspond to (if we can call it this way) the best adjustment of the diffusion model to the data points: for fibers that displayed either a secondary decaying or rising phase of $[Mg^{2+}]_i$, only the

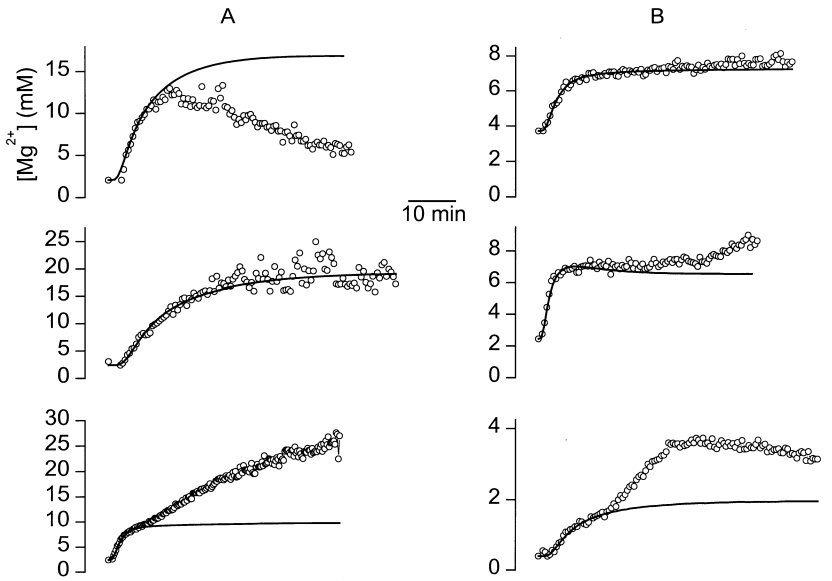

Fig. 6. Heterogeneity of the time course of change in $[Mg^{2+}]_i$ following a Mg-pidolate injection, in fibers that were either partially free of silicone (panel a) or completely free of silicone (panel b). The continuous curve superimposed to each series of data points corresponds to the best attempt of fitting the diffusion model to the initial change in $[Mg^{2+}]_i$ (see text for details). In panel a, from top to bottom, fibers length (l) and distance between injection site and measurement site (d) were 1125 μm, 1190 μm, 760 μm, and 750 μm, 750 μm and 390 μm, respectively. Superimposed diffusion profiles were calculated with D_{app} values of 250 $\mu m^2\ s^{-1}$, 160 $\mu m^2\ s^{-1}$ and 170 $\mu m^2\ s^{-1}$, respectively. Corresponding values for h were 75 μm, 90 μm and 24 μm. In panel b, from top to bottom, l and d were 975 μm, 1200 μm, 1280 μm, and 500 μm, 500 μm and 780 μm, respectively. Superimposed diffusion profiles were calculated with D_{app} values of 170 $\mu m^2\ s^{-1}$, 290 $\mu m^2\ s^{-1}$ and 230 $\mu m^2\ s^{-1}$, and h values of 15 μm, 22 μm and 9 μm, respectively.

initial change in $[Mg^{2+}]_i$ was used. Values for D_{app} corresponding to these fits were within the same range as estimated from fully insulated fibers, ranging between 155 and 250 $\mu m^2\ s^{-1}$ ($n = 9$). Fig. 6b shows $[Mg^{2+}]_i$ changes following a magnesium injection in three silicone-free fibers. Again, the pattern of change in $[Mg^{2+}]_i$ was variable, being either compatible with diffusion (first row) or displaying a secondary rising phase (middle and lower rows). From top to bottom, the curves superimposed to the data points were calculated with D_{app} values of 170, 290 and 230 $\mu m^2\ s^{-1}$.

4.4. Mag-indo-1 and Ca^{2+} diffusion in fully insulated fibers

In order to compare our estimate of the Mg^{2+} diffusion coefficient value in skeletal muscle fibers with that of other diffusing species of interest, a few experiments were performed to measure mag-indo-1 and Ca^{2+} diffusion using similar procedures as used for Mg^{2+} (Section 2). One other goal was that, since values for the diffusion coefficient for Ca^{2+} ions and for fluorescent dyes similar to mag-indo-1 are available in the literature, we could compare our estimations with these values and hopefully, further validate our modeling procedure. Fig. 7a shows the time-dependent changes in fluorescence at 405 nm (open squares) and 470 nm (open circles) due to a mag-indo-1 microinjection performed within one end of a fully insulated muscle fiber. Fluorescence was measured at the other end of the fiber, 1250 μm away from the injection site. As dye diffused from the injection site to the measurement site, fluorescence gradually increased at both wavelengths. In Fig. 7b, fluorescence data points at 405 nm were normalized so as to reach the same maximum amplitude as the F_{470} data points, at the end of the series. The time course of change in fluorescence was very similar at both wavelengths, indicating that the increase in dye concentration was mostly responsible for the observed changes in fluorescence with little, if any, interference from $[Mg^{2+}]_i$ changes. In Fig. 7b the line superimposed to the data points corresponds to the best fit of the diffusion model to the experimental

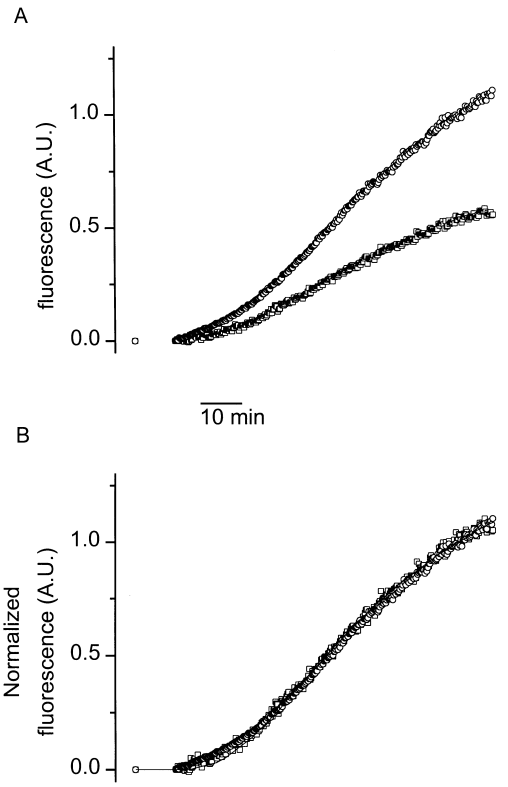

Fig. 7. Mag-indo-1 diffusion in a fully insulated muscle fiber. Panel a shows the increase in fluorescence at 405 (open squares) and 470 nm (open circles) measured at one end of the fiber, 1250 μm away from the mag-indo-1 injection site located at the other end of the fiber. In b, fluorescence data were normalized to the same maximum amplitude and the superimposed continuous line shows the diffusion profile calculated with a diffusion coefficient of 58 $\mu m^2\ s^{-1}$.

data. It was achieved with a dye diffusion coefficient of 58 $\mu m^2\ s^{-1}$. Similar experiments performed in two other fibers yielded a dye diffusion coefficient of 50 and 72 $\mu m^2\ s^{-1}$. Under our experimental conditions, mag-indo-1 diffusion thus appears to proceed at a rate approximately three times lower than that of Mg^{2+}. Fig. 8 shows the result of a Ca^{2+} diffusion experiment. The fiber was 925 μm long and the distance between the injection site and the measurement site was 500 μm. Following the $CaCl_2$ injection within one end of the fiber, $[Ca^{2+}]_i$ slowly increased with a diffusion rate estimated to 18 $\mu m^2\ s^{-1}$ (superimposed curve). The actual change in free cal-

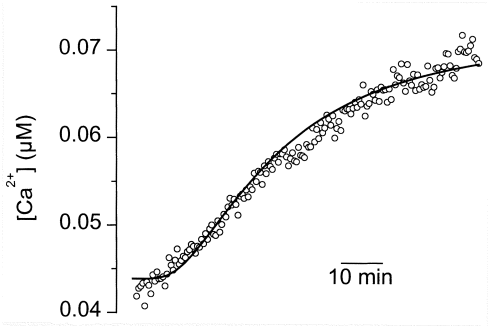

Fig. 8. Ca^{2+} diffusion in a fully insulated fiber loaded with indo-1. A solution containing 20 mM $CaCl_2$ was injected within one end of the fiber and indo-1 fluorescence was measured 500 μm from the injection site (see text for details). The graph shows the calculated $[Ca^{2+}]_i$ change produced by the $CaCl_2$ injection. The superimposed curve corresponds to the Ca^{2+} diffusion profile calculated with a diffusion coefficient of 18 $\mu m^2\ s^{-1}$.

cium concentration was very small, increasing from an initial level of ~45 nM up to ~70 nM at the end of the records. A similar result was obtained in one other fiber, yielding a Ca^{2+} diffusion coefficient of 20 $\mu m^2\ s^{-1}$.

4.5. In vitro diffusion of mag-indo-1 and Mg^{2+}

Fig. 9a shows the time course of fluorescence changes at 405 and 470 nm measured in a capillary tube following a mag-indo-1 'injection', as described in Section 2 (in vitro measurements). The capillary tube was 1180 μm long and the measurement site was 730 μm away from the 'injection' site. Fluorescence data at the two wavelengths were normalized to the same maximum amplitude. The line superimposed to the data points corresponds to the diffusion profile calculated with a diffusion coefficient of 530 $\mu m^2\ s^{-1}$. Data from another capillary tube gave a value of 480 $\mu m^2\ s^{-1}$. Fig. 9b shows the change in $[Mg^{2+}]$ induced by a Mg-pidolate 'injection' in a mag-indo-1 containing capillary tube (see Section 2). The tube was ~4400 μm long and the mea-

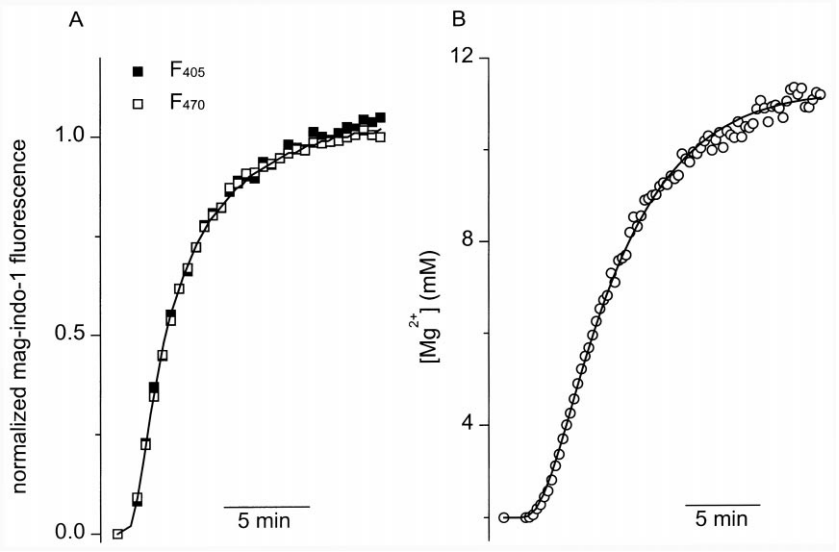

Fig. 9. In vitro diffusion of mag-indo-1 (a) and Mg^{2+} (b). Panel a shows normalized intensities of fluorescence at 405 nm (filled symbols) and 470 nm (open symbols) measured in a glass capillary tube, following a mag-indo-1 'injection' performed within one end of the tube. Tube length was 1180 μm and distance from the injected end to measurement site was 730 μm. The superimposed diffusion profile (continuous line) was calculated with a diffusion coefficient of 530 $\mu m^2\ s^{-1}$. Panel b shows the result of an Mg^{2+} diffusion experiment performed in a 4410 μm long capillary tube. Distance between the 'injected' capillary end and the fluorescence measurement site was 1450 μm. The superimposed Mg^{2+} diffusion profile was calculated with a diffusion coefficient of 730 $\mu m^2\ s^{-1}$ and a h value of 125 μm (see text for details).

surements were taken 1450 μm away from the 'injected' end. The diffusion coefficient calculated from the modeling (superimposed line) was 730 $\mu m^2\ s^{-1}$. The mean value from five capillary tubes was $690 \pm 30\ \mu m^2\ s^{-1}$, which is consistent with the value given in Lide [16]: 706 $\mu m^2\ s^{-1}$ at 25°C.

5. Discussion

5.1. Mg^{2+} diffusion in insulated muscle fibers

The present work shows that Mg^{2+} diffuses readily within isolated skeletal muscle fibers. The value of the apparent Mg^{2+} longitudinal diffusion coefficient is $\sim 190\ \mu m^2\ s^{-1}$, which is 0.27 times the one estimated in vitro. This ratio is twice less than the one reported for Na^+, SO_4^{2-} and K^+ ions and also for non-electrolytes such as sorbitol and sucrose, in skinned frog skeletal muscle fiber [17], indicating that myoplasmic Mg^{2+} apparent diffusion rate is twice reduced as compared to that of these other species. Since the diffusion coefficient is inversely proportional to the viscosity and to the hydrodynamical radius of the moving ion (Stokes law), both the increased viscosity of the cytoplasm as compared to water, and the increase of size of the ion in the cytoplasm (due for instance to hydratation), have to be considered. Concerning the first point, it is well known that, due to high macromolecular concentrations, the cytoplasmic viscosity is ~ 2 centipoise [18,19]. Therefore, viscosity effects should be expected to account for a factor of ~ 2 in the reduction of D_{Mg}, as previously observed for the diffusion rate of other ionic species [17]. A change of hydratation or in shape of the moving ions is unlikely to occur in the cellular cytoplasm. The Mg^{2+} ion is hydrated in aqueous solutions with six water molecules: at high ionic strengths such as in cytoplasm, the electrostatic ion–dipole bonds are screened by counter-ions, and therefore less probable to occur. Moreover, from Debye–Hückel theory, the radius of the counter-ion cloud (involved in the hydrodynamic radius) is inversely proportional to the square root of the ionic strength. Consequently, the hydrodynamic radius should be smaller in the cytoplasm than in dilute salt solutions. From our in vitro value of 690 $\mu m^2\ s^{-1}$ it seems thus reasonable to consider that, taking into account the effects of viscosity, the cytoplasmic D_{Mg} value is $\sim 350\ \mu m^2\ s^{-1}$.

To account for the remaining two factors in diffusion coefficient reduction, reversible binding of Mg^{2+} ions to cytoplasmic binding sites has to be considered [10,15].

Wagner and Keizer [10] investigated models of Ca^{2+} diffusion taking into account the effects of both mobile and non-mobile binding sites. They showed that ion binding to mobile sites can either increase or decrease the ion diffusion speed, depending on the relative mobilities of the ion and of the sites. This was experimentally confirmed by Gabso et al. [9] who observed an increased Ca^{2+} diffusion coefficient in axons of cultured Aplysia neurons due to the indicator fura-2, the mobility of which was higher than that of Ca^{2+}. Under our experimental conditions, since the value of the mag-indo-1 diffusion coefficient is smaller than the value of the Mg^{2+} diffusion coefficient, Mg^{2+} binding to the indicator may slow down the Mg^{2+} diffusion speed.

According to Wagner and Keizer [10], in the presence of mobile and non-mobile buffers, the apparent Mg^{2+} diffusion coefficient is given by:

$$D_{app} = \beta \times (D_{Mg} + \Sigma\gamma_m \times D_{MgLm}) \tag{5}$$

with

$$\frac{1}{\beta} = 1 + \Sigma\frac{K_{am} \times [L_{Tm}]}{[1 + K_{am} \times [Mg]]^2} + \Sigma\frac{K_{as} \times [L_{Ts}]}{[1 + K_{as} \times [Mg]]^2} = 1 + \Sigma\gamma_m + \Sigma\gamma_s \tag{6}$$

with MgL, Mg, L_T, and K_a, referring to ligand-bound magnesium, free magnesium, total binding sites, and association constant of the binding reaction, respectively. Subscript *s* and *m* refer to static and mobile ligands, respectively.

These equations are valid for several static and mobile ligands, under the assumptions that ligands are homogeneously distributed throughout

the diffusing volume, that binding is much faster than any diffusion process, and that free and Mg-bound mobile ligands have the same mobilities. If we first neglect the effects of static buffers, one can look at the importance of the mobile term $\Sigma\gamma_m \times D_{\mathrm{MgLm}}$ in Eq. (5) as compared to D_{Mg}. Inside the fiber, the main Mg^{2+} mobile ligands are ATP, inorganic phosphate, phosphocreatine, to which should be added the fluorescent dye mag-indo-1.

Concerning ATP, assuming a total concentration of 6 mM and an association constant for Mg^{2+} of 13.5 mM^{-1} [20], ATP can be considered as fully saturated at the resting Mg^{2+} levels measured here, and it should thus not influence Mg^{2+} diffusion along the cell.

Phosphocreatine (Pc) is highly concentrated inside the muscle cells (25 mM) and its K_{am} for Mg^{2+} is given as 0.02 mM^{-1} [20]. The corresponding γ_m value is 0.45 at the resting Mg^{2+} level measured here (2.4 mM), and less for higher concentrations. With a D_{MgLm} value for phosphocreatine of 330 $\mu m^2\ s^{-1}$ [21], the corresponding $\gamma_m \times D_{\mathrm{MgLm}}$ term reaches a maximum value of 150 $\mu m^2\ s^{-1}$.

Concerning inorganic phosphate (Pi), with a K_{am} of 0.06 mM^{-1} and a total concentration of 4 mM [20], the same calculation as above gives a corresponding γ_m value of 0.18 at the resting $[Mg^{2+}]$ level and smaller during the diffusion process. Assuming a diffusion coefficient of 500 $\mu m^2\ s^{-1}$ (computed, in the absence of published data, from phosphocreatine D value [20], multiplied by the cubic root of the ratio of molecular weights Pc/Pi), the $\gamma_m \times D_{\mathrm{MgLm}}$ term for inorganic phosphate is 90 $\mu m^2\ s^{-1}$ in resting conditions.

For the mag-indo-1 probe, we measured a D_{MgLm} value of $\sim 60\ \mu m^2\ s^{-1}$, while the mag-indo-1 association constant K_{am} for Mg^{2+} is $\sim 0.2\ mM^{-1}$ [6]. Under our experimental conditions, considering a mag-indo-1 concentration of 0.2 mM, the corresponding γ_m value can be calculated at any Mg^{2+} concentration: γ_m is very low at high Mg^{2+} concentrations in the vicinity of the initial magnesium pulse, and it increases as Mg^{2+} diffuses within the cell. At the mean resting Mg^{2+} level measured here, the value for γ_m is ~ 0.03, and consequently, the $\gamma_m \times D_{\mathrm{MgLm}}$ term for mag-indo-1 is less than $\sim 2\ \mu m^2\ s^{-1}$, negligible as compared to the measured apparent Mg^{2+} diffusion coefficient (190 $\mu m^2\ s^{-1}$).

If one only considers the known, above described, mobile Mg^{2+} buffers, $\frac{1}{\beta}$ can be calculated as $1 + \Sigma\gamma_m$ which gives a value of ~ 1.65. Under these conditions, using Eq. (5) with a D_{Mg} of 350 $\mu m^2\ s^{-1}$ (which takes into account the effect of cytoplasmic viscosity), one can calculate a D_{app} value of 360 $\mu m^2\ s^{-1}$, similar to D_{Mg}. Consequently, the known Mg^{2+} mobile buffers cannot be expected to significantly influence the Mg^{2+} diffusion coefficient within the cytoplasm.

In order to explain the reduced value of D_{app} (190 $\mu m^2\ s^{-1}$), it is necessary to consider the effect of static Mg^{2+} ligands. Each static ligand will account for a γ_s term in Eq. (6), so decreasing the value of β, and consequently decreasing the value of the ratio D_{Mg} over D_{app}. For instance, Mg^{2+} binding sites to parvalbumin could be considered. Due to its shape and weight parvalbumin can be considered as static as compared to small ions. However, with a total concentration of parvalbumin binding sites of 0.7 mM and an association constant of $\sim 5.2\ mM^{-1}$ [22] the corresponding γ_s term is very small (~ 0.02) at the resting Mg^{2+} levels measured here. Mg^{2+} binding to parvalbumin should thus not affect the Mg^{2+} diffusion rate.

In order to explain the measured value of D_{app}, it is necessary to consider that there are other non-mobile cytoplasmic Mg^{2+} buffers, the identity of which can only be speculative. To be responsible for the decrease in Mg^{2+} diffusion rate from 350 $\mu m^2\ s^{-1}$ to 190 $\mu m^2\ s^{-1}$, these sites should exhibit Mg^{2+} binding properties corresponding to a $\Sigma\gamma_s$ value of ~ 1.45. If a single population of such sites was to be involved, this could, for instance, correspond to a total concentration of sites of ~ 40 mM with an affinity constant of $\sim 0.05\ mM^{-1}$.

Table 1 summarizes the results from our measurements of diffusion coefficients for Mg^{2+}, Ca^{2+} and mag-indo-1. The reduction of D_{Mg} in the myoplasm as compared to the in vitro conditions is far less dramatic than what we observed for

Table 1
Diffusion coefficients for Mg^{2+}, Ca^{2+} and mag-indo-1

	Diffusion coefficient ($\mu m^2\ s^{-1}$)	
	In vivo	In vitro
Mg^{2+}	188 ± 9 ($n = 16$)	690 ± 30 ($n = 5$)
Ca^{2+}	18, 20	790[a]
mag-indo-1	50, 58, 72	480, 530

[a][25], all measured values are given when less than four experiments were performed.

mag-indo-1 and a fortiori for Ca^{2+} ions. In the capillary tubes the mag-indo-1 diffusion coefficient was $\sim 500\ \mu m^2\ s^{-1}$, a value which is consistent with its size (439 mol. wt. for the tetra-valent form) [17]. In comparison, within the muscle fibers, the mean mag-indo-1 diffusion coefficient was $60 \pm 6\ \mu m^2\ s^{-1}$ ($n = 3$). This value is similar to the one reported by Konishi et al. [23] in frog muscle fibers for furaptra, a Mg^{2+}-sensitive fluorescent dye with a size similar to mag-indo-1, although these measurements were performed at a temperature of 16°C. Under our conditions, myoplasmic mag-indo-1 diffusion appears to be reduced to a greater extent (by a factor of ~ 8 with respect to a salt buffer) as compared to the results obtained with furaptra, where the reduction was only by a factor of ~ 4 [23]. This likely indicates that under our experimental conditions, mag-indo-1 is heavily bound to myoplasmic constituents of low mobility [24].

The Ca^{2+} diffusion coefficient has previously been reported to be very much lower in frog skeletal muscle fibers than in free solution [17]. In two fibers, following a $CaCl_2$ injection, we could observe a change in intracellular $[Ca^{2+}]$ displaying a time course consistent with an apparent diffusion coefficient of $\sim 20\ \mu m^2\ s^{-1}$, a value 40 times lower than measured in free solution [25]. Of course, this value is likely to be overestimated since, as experimentally demonstrated by Gasbo et al. [9], the presence of a high affinity calcium indicator is expected to speed up Ca^{2+} diffusion. In any case, our results at least confirm the heavy slowing of Ca^{2+} diffusion within muscle fibers [17], an effect that is obviously related to the high intrinsic calcium buffering capacity of this preparation. More evidence for it is the tiny level of measured $[Ca^{2+}]$ change (tens of nanomoles) whereas millimolar levels were likely to be present at the injection site. This property is definitely not shared by Mg^{2+} which under the same conditions diffuses 10 times faster than Ca^{2+}.

The determination of the Mg^{2+} diffusion coefficient within muscle fibers has significant relevance regarding the interpretation of earlier data obtained in our laboratory: in a previous work, we showed that the amplitude distribution of the changes in $[Mg^{2+}]_i$ brought by influxes of Mg^{2+} through the nicotinic receptors, appeared inconsistent with what was expected from a simple cytoplasmic Mg^{2+} buffering mechanism [6]. This led us to suspect that Mg^{2+} diffusion within the cytoplasm could be very slow, leading to local cytoplasmic Mg^{2+} accumulation and saturation of the dye. Data from the present work do not support this hypothesis.

5.2. Mg^{2+} diffusion in partially insulated and in silicone free muscle fibers

From the observed time course of $[Mg^{2+}]_i$ change, we found no clear evidence that under conditions more physiological than the full silicone insulation, the muscle fibers were able to rapidly regulate the increase in $[Mg^{2+}]_i$ produced by the magnesium injection. As specified in Section 4, only two fibers, that were partially free of silicone, displayed a late decrease in $[Mg^{2+}]_i$ that followed the initial rise, which could be speculated to indicate that a mechanism operates to bring $[Mg^{2+}]_i$ back to the resting level. Other fibers either displayed similar results as fully insulated fibers or showed a secondary increasing phase of $[Mg^{2+}]_i$. Since mag-indo-1 is also sensitive to Ca^{2+} ions, we considered the possibility that this last observation could be due to a rise in cytoplasmic Ca^{2+}, though its origin would be quite obscure. However, a rough approximation indicates that the amplitude of secondary phases such as shown in Fig. 6 could correspond to more than 10% of a change in mag-indo-1 saturation. Assuming the mag-indo-1 affinity for Ca^{2+} ions to be of the order of 30 μM [26], this would correspond to a change in $[Ca^{2+}]_i$ of a few micromolar,

likely to be accompanied by a contraction of the cell, which was not observed. Overall, the observed heterogeneity of responses has to be taken as evidence that, in fibers that were not fully embedded within silicone, some yet unidentified processes that may be of critical importance for intracellular Mg^{2+} regulation, do operate.

Acknowledgements

We thank Drs B. Allard and O. Rougier for comments on the manuscript. We are grateful to Drs C. Chouabe and M. Fatemi who helped us to obtain the rat muscles. This study was supported by the Centre National de la Recherche Scientifique (CNRS) and the University Claude Bernard.

References

[1] P.R. Stanfield, Intracellular Mg^{2+} may act as a co-factor in ion channel function, Trends Neurosci. 81 (1988) 475–476.
[2] A. Romani, A. Scarpa, Regulation of cell magnesium, Arch. Biochem. Biophys. 298 (1992) 1–12.
[3] M. Konishi, Cytoplasmic free concentrations of Ca^{2+} and Mg^{2+} in skeletal muscle fibers at rest and during contraction, Jpn. J. Physiol. 48 (1998) 421–438.
[4] M. Konishi, N. Suda, S. Kurihara, Fluorescence signals from the Mg^{2+}/Ca^{2+} indicator furaptra in frog skeletal muscle fibers, Biophys. J. 64 (1993) 223–239.
[5] L.A. Blatter, Intracellular free magnesium in frog skeletal muscle studied with a new type of magnesium-selective microelectrode: interactions between magnesium and sodium in the regulation of $[Mg]_i$, Pflügers Arch. 416 (1990) 238–246.
[6] L. Csernoch, J.C. Bernengo, P. Szentesi, V. Jacquemond, Measurements of intracellular Mg^{2+} concentration in mouse skeletal muscle fibers with the fluorescent indicator mag-indo-1, Biophys. J. 75 (1998) 957–967.
[7] N.L. Allbriton, T. Meyer, L. Stryer, Range of messenger action of calcium ion and inositol 1,4,5-trisphospate, Science 258 (1992) 1812–1815.
[8] N.F. Al-Baldawi, R.F. Abercrombie, Calcium diffusion coefficient in *Myxicola axoplasm*, Cell Calcium 17 (1995) 422–430.
[9] M. Gabso, E. Neher, M.E. Spira, Low mobility of the Ca^{2+} buffers in axons of cultured Aplysia neurons, Neuron 18 (1997) 473–481.
[10] J. Wagner, J. Keizer, Effects of rapid buffers on Ca^{2+} diffusion and Ca^{2+} oscillations, Biophys. J. 67 (1994) 447–456.
[11] V. Jacquemond, Indo-1 fluorescence signals elicited by membrane depolarization in enzymatically isolated mouse skeletal muscle fibers, Biophys. J. 73 (1997) 920–928.
[12] C. Collet, B. Allard, Y. Tourneur, V. Jacquemond, Intracellular calcium signals measured with indo-1 in isolated skeletal muscle fibres from control and *mdx* mice, J. Physiol. (Lond.) 520 (1999) (1999) 417–429.
[13] G. Grynkiewicz, M. Poenie, R.Y. Tsien, A new generation of Ca^{2+} indicators with greatly improved fluorescence properties, J. Biol. Chem. 260 (1985) 3440–3450.
[14] J. Crank, The mathematics of diffusion, 6th ed, Oxford University Press, London, 1978.
[15] A. Zador, C. Koch, Linearized models of calcium dynamics: formal equivalence to the cable equation, J. Neurosci. 14 (1994) 4705–4715.
[16] D.R. Lide, Ionic conductivity and diffusion at infinite dilution, in: Lide D.R. (Ed.), CRC Handbook of Chemistry and Physics, 79th ed, CRC Press, Boca Raton, FL, 1998.
[17] M.J. Kushmerick, R.J. Podolsky, Ionic mobility in muscle cells, Science 166 (1969) 1297–1298.
[18] A.M. Mastro, A.D. Keith, Diffusion in the aqueous compartment, J. Cell. Biol. 99 (1984) 180–187.
[19] N. Periasamy, M. Armijo, A.S. Verkman, Picosecond rotation of small polar fluorophores in the cytosol of sea urchin eggs, Biochemistry 30 (1991) 11836–11841.
[20] H. Westerblad, D.G. Allen, Myoplasmic free Mg^{2+} concentration during repetitive stimulation of single fibres from mouse skeletal muscle, J. Physiol. (Lond.) 453 (1992) 413–434.
[21] M.J. Hubley, B.R. Locke, T.S. Moerland, Reaction-diffusion analysis of the effects of temperature on high-energy phosphate dynamics in goldfish skeletal muscle, J. Exp. Biol. 200 (1997) 975–988.
[22] J. Garcia, M.F. Schneider, Calcium transients and calcium release in rat fast-twitch skeletal muscle fibres, J. Physiol. (Lond.) 463 (1993) 709–728.
[23] M. Konishi, S. Hollingworth, A.B. Harkins, S.M. Baylor, Myoplasmic calcium transients in intact frog skeletal muscle fibers monitored with the fluorescent indicator furaptra, J. Gen. Physiol 97 (1991) 271–301.
[24] M. Konishi, S.M. Baylor, Myoplasmic calcium transients monitored with purpurate indicator dyes injected into frog skeletal muscle fibers, J. Gen. Physiol. 97 (1991) 245–270.
[25] J.H. Wang, Tracer diffusion in liquids. IV Self diffusion of calcium ions and chloride ions in aqueous calcium chloride solutions, J. Am. Chem. Soc. 75 (1953) 1769–1770.
[26] R.P. Haugland, Handbook of Fluorescent Probes and Research Chemicals, 6th ed, Molecular Probes, Eugene, OR, 1996.